Nanostructures

International Edition: DOI: 10.1002/anie.201502117
German Edition: DOI: 10.1002/ange.201502117

Ultrathin MoS_2 Nanosheets Supported on N-doped Carbon Nanoboxes with Enhanced Lithium Storage and Electrocatalytic Properties

*Xin-Yao Yu, Han Hu, Yawen Wang, Hongyu Chen, and Xiong Wen (David) Lou**

Abstract: *Molybdenum disulfide (MoS_2) has received considerable interest for electrochemical energy storage and conversion. In this work, we have designed and synthesized a unique hybrid hollow structure by growing ultrathin MoS_2 nanosheets on N-doped carbon shells (denoted as C@MoS_2 nanoboxes). The N-doped carbon shells can greatly improve the conductivity of the hybrid structure and effectively prevent the aggregation of MoS_2 nanosheets. The ultrathin MoS_2 nanosheets could provide more active sites for electrochemical reactions. When evaluated as an anode material for lithium-ion batteries, these C@MoS_2 nanoboxes show high specific capacity of around 1000 mAh g^{-1}, excellent cycling stability up to 200 cycles, and superior rate performance. Moreover, they also show enhanced electrocatalytic activity for the electrochemical hydrogen evolution.*

Hollow nanostructured metal oxides/sulfides as an important family of functional materials are of great interest in recent years.[1–4] In particular, the presence of a well-defined interior void with functional shells endows them with potential applications in energy conversion and storage.[3,5–8] For example, Wang and co-workers have synthesized several kinds of multishelled metal oxides hollow microspheres and investigated their interesting shell-number-dependent properties in lithium-ion batteries (LIBs) and dye-sensitized solar cells.[3,5,9] We have recently developed a simple sacrificial template method to synthesize uniform $Ni_xCo_{3-x}S_4$ hollow nanoprisms with tunable composition which exhibit excellent pseudocapacitive properties.[8] Despite the great advances, the intrinsic poor electronic/ionic conductivity of metal oxides/sulfides severely limits their practical application in energy conversion and storage devices.

Molybdenum disulfide (MoS_2), a representative layered two-dimensional (2D) material, has received considerable attention in energy conversion and storage.[10–19] MoS_2 has been suggested as a promising anode material for LIBs because it can deliver very high specific capacities.[12–14] However, the capacity fading and poor rate performance greatly limit their application. To address these issues, various strategies have been proposed to improve the electrochemical performance of MoS_2 by broadening the interlayer distance of MoS_2, tuning the morphology at nanoscale or using carbonaceous materials as the conductive matrix.[3,15,20–28] On the other hand, MoS_2-based electrocatalysts have been considered as promising alternatives for platinum for the hydrogen evolution reaction (HER).[3,11,16] Increasing the number of exposed active sites on the edges and improving the electrical conduction by choosing suitable conductive substrates are two effective methods to enhance the electrocatalytic efficiency of MoS_2.[11,16,29,30]

Herein, we report the rational design and synthesis of a novel nanosheets-on-box nanostructure composed of ultrathin MoS_2 nanosheets on N-doped carbon nanoboxes designated as C@MoS_2 nanoboxes. As expected, when evaluated as an anode material for LIBs, these C@MoS_2 nanoboxes manifest high specific capacity of around 1000 mAh g^{-1}, excellent cycling stability up to 200 cycles, and superior rate performance. Moreover, they also show enhanced electrocatalytic activity for the electrochemical HER.

The multistep synthesis process for the C@MoS_2 nanoboxes is illustrated in Figure 1. Very uniform α-Fe_2O_3 nanocubes with an average size of about 500 nm (Figure S1 a and b in the Supporting Information) synthesized by a facile coprecipitation method[31] are used as templates to synthesize N-doped carbon nanoboxes. In the first step, Fe_2O_3 nanocubes are successfully coated with a uniform and smooth layer of polydopamine (PDA) with a thickness of around 40 nm (Figure S1 c and d). In step II, these core–shell Fe_2O_3@PDA nanocubes are transformed into Fe_3O_4@C nanocubes after carbonization in N_2 (Figure S2).[32] The Fe_3O_4 core can be easily dissolved by HCl to obtain carbon nanoboxes (step III). Lastly, a layer of ultrathin MoS_2 nanosheets is successfully grown on the surface of carbon nanoboxes through a facile

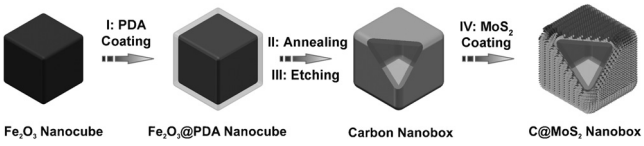

Figure 1. Illustration of the synthesis process of C@MoS_2 nanoboxes.

[*] Dr. X. Y. Yu, Dr. H. Hu, Prof. X. W. Lou
School of Chemical and Biomedical Engineering
Nanyang Technological University
62 Nanyang Drive, Singapore 637459 (Singapore)
E-mail: xwlou@ntu.edu.sg
davidlou88@gmail.com
Homepage: http://www.ntu.edu.sg/home/xwlou/
Dr. X. Y. Yu
Nano-materials and Environment Detection Laboratory
Hefei Institutes of Physical Science, Chinese Academy of Sciences
Hefei 230031 (P.R. China)
Y. W. Wang, Prof. H. Y. Chen
Division of Chemistry and Biological Chemistry
Nanyang Technological University
Singapore 637371 (Singapore)

Supporting information for this article is available on the WWW under http://dx.doi.org/10.1002/anie.201502117.

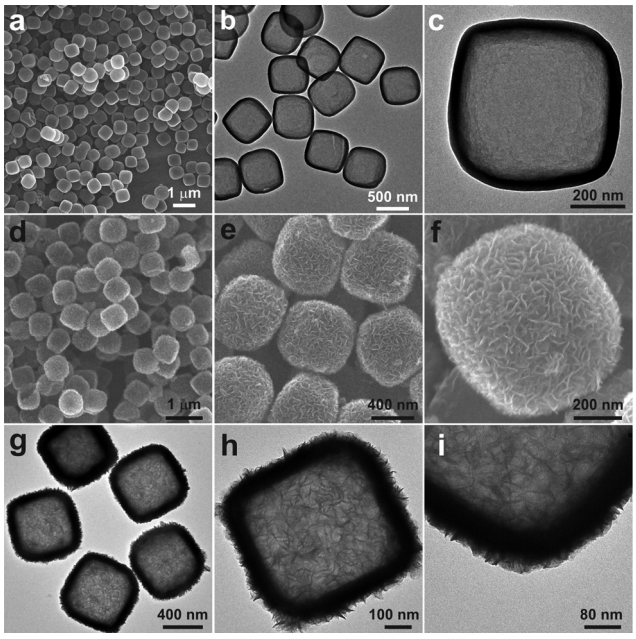

Figure 2. FESEM (a) and TEM (b,c) images of carbon nanoboxes, and FESEM (d–f) and TEM (g–i) images of C@MoS_2 nanoboxes.

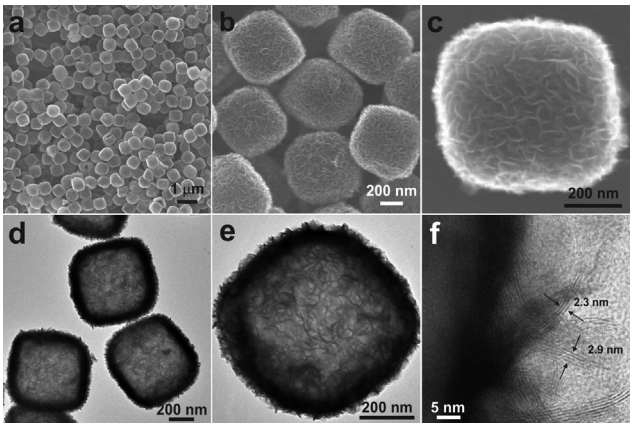

Figure 3. FESEM (a–c) and TEM images (d–f) of C@MoS_2 nanoboxes after annealing in H_2 at 700 °C for 2 h.

solvothermal method, leading to the formation of C@MoS_2 nanoboxes (step IV).

As shown in the low-magnification field-emission scanning electron microscopy (FESEM) image in Figure 2 a, the carbon nanoboxes obtained are also very uniform with an average size of about 580 nm. The hollow interior of carbon nanoboxes is further elucidated by transmission electron microscopy (TEM) (Figure 2 b,c). The obtained carbon nanoboxes are dispersed in *N*,*N*-dimethylformamide (DMF) solvent for further growth of MoS_2 nanosheets. The X-ray powder diffraction (XRD) pattern of the obtained product is quasi-amorphous (Figure S3).[11] After the solvothermal process, the surface of carbon nanoboxes is uniformly covered with MoS_2 nanosheets (Figure 2 d,e). The thickness of the MoS_2 shell is about 35 nm. The magnified FESEM image reveals that the MoS_2 layer is randomly assembled by ultrathin nanosheets (Figure 2 f). TEM images (Figure 2 g–i) confirm the same structural features as shown by the above FESEM observations. It is worth noting that there is no visible interlayer gap observed between the carbon shell and the MoS_2 layer (Figure 2 i), indicating that the MoS_2 nanosheets are strongly anchored on the carbon nanoboxes. This can be ascribed to the strong interactions between the functional groups on carbon nanoboxes and the Mo precursor. The uniformly distributed functional groups on carbon nanoboxes could not only provide growing sites for MoS_2 but also prevent the aggregation of formed particles. In the absence of carbon nanoboxes, severely aggregated nanosheets-assembled particles are produced (Figure S4).

The as-obtained C@MoS_2 nanoboxes are further annealed at 700 °C in H_2 for 2 h to obtain highly crystalline MoS_2 nanosheets. All of the diffraction peaks of the annealed product can be perfectly assigned to hexagonal MoS_2 (JCPDS card no. 37-1492; Figure S3). The (002) diffraction peak is shifted to a lower angle of 14.17° compared to the standard angle of 16.71°, indicating an expansion of the interlayer distance.[23] The FESEM and TEM images in Figure 3 a–e show that the nanosheets-on-box nanostructure is perfectly retained. A high-resolution TEM image demonstrates that each MoS_2 nanosheet is composed of three to five layers only (Figure 3 f). The interlayer distance (0.66 nm) of MoS_2 on carbon nanoboxes is larger than that of natural MoS_2 (0.62 nm), further verifying the expanded interlayer spacing. This may be attributed to the substrate effect and the ultrathin feature of the MoS_2 nanosheets, leading to formation of an undulated structure.[23] Raman spectra further demonstrate the few-layered ultrathin nature of MoS_2 nanosheets on carbon nanoboxes (Figure S5).[33] X-ray photoelectron spectroscopy (XPS) measurements confirm that the annealed C@MoS_2 nanoboxes contain Mo, S, C, N, and O (Figure S6 a). The binding energies of Mo $2d_{5/2}$ and Mo $2d_{3/2}$ peaks are located at 225.8 and 228.9 eV, respectively, which confirms the Mo^{4+} state of Mo in MoS_2 (Figure S6 b). The binding energies at 162.6 and 163.8 eV in the S 2p spectrum are attributed to the S^{2-} of MoS_2 (Figure S6 c). The high-resolution XPS spectra of C 1s and N 1s verify the successful doping of N in the carbon nanoboxes (Figure S6 d,e). The O 1s spectrum confirms the existence of oxygen-containing functional groups (Figure S7). As determined by thermogravimetric analysis, the content of MoS_2 in the nanocomposite is approximately 82 wt % (Figure S8). In virtue of the hollow nanostructure and ultrathin nanosheets, these annealed C@MoS_2 nanoboxes possess a large specific surface area of 123.7 $m^2 g^{-1}$, which is higher than that of annealed bare MoS_2 (82.2 $m^2 g^{-1}$; Figure S9).

The lithium storage properties of annealed C@MoS_2 nanoboxes are first evaluated by cyclic voltammetry (CV) (Figure S10). In the first cycle, the strong cathodic peak at ca. 1.07 V can be assigned to the insertion of Li^+ ions into the interlayer MoS_2 lattice to form Li_xMoS_2, whereas the other peak at ca. 0.54 V is due to a further reaction between Li_xMoS_2 and Li^+, resulting in the formation of metallic Mo nanoparticles and Li_2S.[12,14,22] In the subsequent anodic scan, a pronounced peak at about 2.34 V can be attributed to the delithiation of Li_2S to sulfur.[10,23] In the following cycles, two

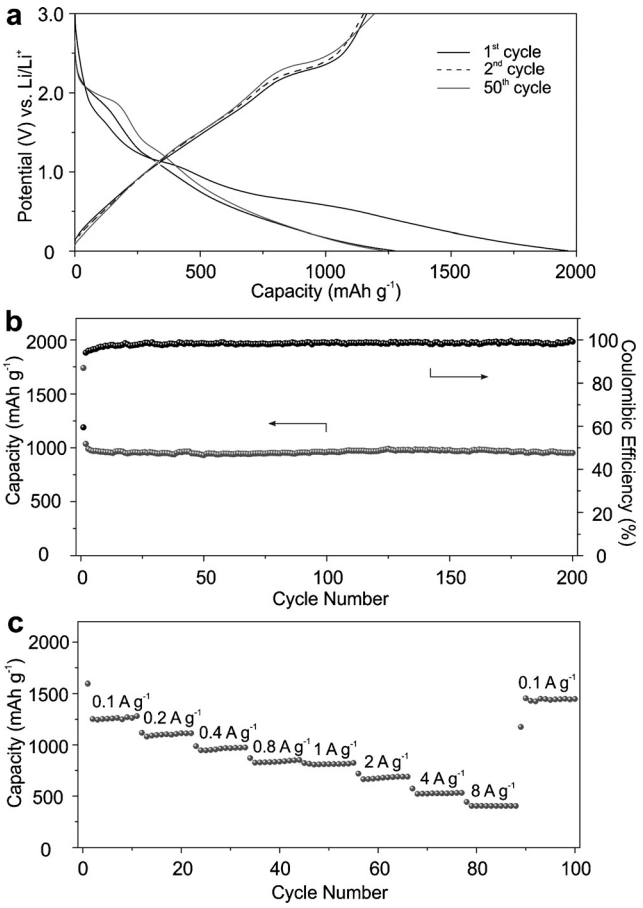

Figure 4. Electrochemical lithium-storage properties of annealed C@MoS_2 nanoboxes: a) discharge–charge voltage profiles for the 1st, 2nd, and 50th cycles at a current density of 0.1 $A g^{-1}$; b) cycling performance at a current density of 0.4 $A g^{-1}$ and the corresponding Coulombic efficiency; c) rate performance at various current rates.

cathodic peaks emerge at around 1.88 and 1.17 V, which are related to a multistep lithium insertion mechanism.[21] Figure 4a shows the representative discharge–charge voltage profiles of the annealed C@MoS_2 nanoboxes at a current density of 0.1 $A g^{-1}$. The C@MoS_2 electrode delivers high first-cycle discharge and charge capacities of 1966 and 1164 $mAh g^{-1}$ respectively, corresponding to a Coulombic efficiency (CE) of 59.2%. The initial loss is mainly caused by the decomposition of electrolyte or some irreversible processes such as the formation of a solid–electrolyte interface layer during the first cycle.[14,21] A discharge capacity of 1274 $mAh g^{-1}$ is delivered in the second cycle, followed by a charge capacity of 1151 $mAh g^{-1}$, giving rise to a high CE of about 93%. The discharge capacity remains at about 1233 $mAh g^{-1}$ after 50 cycles at a current rate of 0.1 $A g^{-1}$ (Figures 4a and S11). Moreover, the C@MoS_2 nanoboxes can be cycled with high stability at higher current densities of 0.4 and 1.0 $A g^{-1}$ (Figures 4b and S12). Remarkably, a reversible capacity of 952 $mAh g^{-1}$ at a current rate of 0.4 $A g^{-1}$ after 200 cycles can still be retained, with CE of almost 100% throughout the cycling (Figure 4b). The structural integrity of C@MoS_2 can still be maintained after charging/discharging for 200 cycles (Figure S13) although the particles become significantly larger due to the formation of a gel-like polymeric layer. The rate capability is evaluated at different current densities ranging from 0.1 to 8 $A g^{-1}$ (Figure 4c). As can be seen, the specific capacities are 1280, 1113, 974, 851, 824, 689, 531, and 403 $mAh g^{-1}$ at current densities of 0.1, 0.2, 0.4, 0.8, 1, 2, 4, and 8 $A g^{-1}$, respectively. When the current density is reduced back to 0.1 $A g^{-1}$, the capacity of the C@MoS_2 electrode quickly recovers to as high as 1448 $mAh g^{-1}$, probably due to the growth of a gel-like polymeric layer and activation of electrode materials.[14,21] The cycling stability and rate performance of these C@MoS_2 nanoboxes are superior to annealed bare MoS_2 (Figure S14). Electrochemical impedance spectroscopy measurements show that C@MoS_2 nanoboxes show a smaller diameter of the high-frequency semicircle than bare MoS_2, indicating smaller solid state interface layer resistance (Figure S15).

In addition, the electrocatalytic activity of these C@MoS_2 nanoboxes for HER is also investigated. Previous reports have shown that amorphous MoS_2 materials generally exhibit higher electrocatalytic activity than crystallized samples.[11,29] As such, another similar nanosheets-on-box architecture is constructed with high-temperature annealed carbon nanoboxes as substrates for amorphous MoS_2 coating (Figure S16). The C@MoS_2 nanoboxes exhibit superior activity over bare MoS_2 in both Tafel slope and cathodic current (Figure S17a,b). A Tafel slope of 55 $mV dec^{-1}$ is obtained for the C@MoS_2 nanoboxes. The C@MoS_2 nanoboxes electrode only requires overpotentials of 165 and 200 mV to give current densities of 10 and 35 $mA cm^{-2}$, respectively. To assess the long-term stability of the C@MoS_2 nanoboxes catalyst, potential sweeps are conducted continuously for 1000 cycles. As can be seen, the polarization curve remains largely unchanged compared to the initial one (Figure S17c).

In summary, a novel hybrid nanostructure of ultrathin MoS_2 nanosheets supported on N-doped carbon nanoboxes has been successfully synthesized. These well-defined C@MoS_2 nanoboxes exhibit enhanced lithium storage and electrocatalytic properties, which could be attributed to their unique structure. Specifically, the N-doped carbon nanoboxes substrate has relatively high conductivity. The hollow structure of carbon nanoboxes and ultrathin building blocks can effectively alleviate the strain caused by the large volume change during cycling. The ultrathin MoS_2 nanosheets possess a high surface area for electrode/electrolyte interface and the diffusion length of electrons and ions can be effectively reduced. All these merits would undoubtedly contribute to the electrochemical performance of the electrode materials, leading to high capacity, long cycle life, and superior rate performance for lithium-ion batteries and low Tafel slope and high cathodic current for hydrogen evolution reaction.

Keywords: lithium-ion batteries · molybdenum disulfide · MoS_2 · water splitting

How to cite: *Angew. Chem. Int. Ed.* **2015**, *54*, 7395–7398
Angew. Chem. **2015**, *127*, 7503–7506

[1] Z. Y. Wang, L. Zhou, X. W. Lou, *Adv. Mater.* **2012**, *24*, 1903–1911.

[2] X. Y. Lai, J. E. Halpert, D. Wang, *Energy Environ. Sci.* **2012**, *5*, 5604 – 5618.
[3] L. Zhang, H. B. Wu, Y. Yan, X. Wang, X. W. Lou, *Energy Environ. Sci.* **2014**, *7*, 3302 – 3306.
[4] J. B. Joo, Q. Zhang, I. Lee, M. Dahl, F. Zaera, Y. D. Yin, *Adv. Funct. Mater.* **2012**, *22*, 166 – 174.
[5] S. M. Xu, C. M. Hessel, H. Ren, R. B. Yu, Q. Jin, M. Yang, H. J. Zhao, D. Wang, *Energy Environ. Sci.* **2014**, *7*, 632 – 637.
[6] G. Q. Zhang, B. Y. Xia, C. Xiao, L. Yu, X. Wang, Y. Xie, X. W. Lou, *Angew. Chem. Int. Ed.* **2013**, *52*, 8643 – 8647; *Angew. Chem.* **2013**, *125*, 8805 – 8809.
[7] J. Y. Wang, N. L. Yang, H. J. Tang, Z. H. Dong, Q. Jin, M. Yang, D. Kisailus, H. J. Zhao, Z. Y. Tang, D. Wang, *Angew. Chem. Int. Ed.* **2013**, *52*, 6417 – 6420; *Angew. Chem.* **2013**, *125*, 6545 – 6548.
[8] L. Yu, L. Zhang, H. B. Wu, X. W. Lou, *Angew. Chem. Int. Ed.* **2014**, *53*, 3711 – 3714; *Angew. Chem.* **2014**, *126*, 3785 – 3788.
[9] Z. H. Dong, H. Ren, C. M. Hessel, J. Y. Wang, R. B. Yu, Q. Jin, M. Yang, Z. D. Hu, Y. F. Chen, Z. Y. Tang, H. J. Zhao, D. Wang, *Adv. Mater.* **2014**, *26*, 905 – 909.
[10] X. Xu, Z. Y. Fan, S. J. Ding, D. M. Yu, Y. P. Du, *Nanoscale* **2014**, *6*, 5245 – 5250.
[11] Y. Yan, X. M. Ge, Z. L. Liu, J. Y. Wang, J. M. Lee, X. Wang, *Nanoscale* **2013**, *5*, 7768 – 7771.
[12] L. C. Yang, S. N. Wang, J. J. Mao, J. W. Deng, Q. S. Gao, Y. Tang, O. G. Schmidt, *Adv. Mater.* **2013**, *25*, 1180 – 1184.
[13] K. Chang, W. X. Chen, *Chem. Commun.* **2011**, *47*, 4252 – 4254.
[14] K. Chang, W. X. Chen, *ACS Nano* **2011**, *5*, 4720 – 4728.
[15] P. P. Wang, H. Y. Sun, Y. J. Ji, W. H. Li, X. Wang, *Adv. Mater.* **2014**, *26*, 964 – 969.
[16] Y. G. Li, H. L. Wang, L. M. Xie, Y. Y. Liang, G. S. Hong, H. J. Dai, *J. Am. Chem. Soc.* **2011**, *133*, 7296 – 7299.
[17] Z. Hu, L. X. Wang, K. Zhang, J. B. Wang, F. Y. Cheng, Z. L. Tao, J. Chen, *Angew. Chem. Int. Ed.* **2014**, *53*, 12794 – 12798; *Angew. Chem.* **2014**, *126*, 13008 – 13012.
[18] G. Z. Sun, J. Q. Liu, X. Zhang, X. W. Wang, H. Li, Y. Yu, W. Huang, H. Zhang, P. Chen, *Angew. Chem. Int. Ed.* **2014**, *53*, 12576 – 12580; *Angew. Chem.* **2014**, *126*, 12784 – 12788.
[19] L. N. Ye, C. Z. Wu, W. Guo, Y. Xie, *Chem. Commun.* **2006**, 4738 – 4740.
[20] X. H. Cao, Y. M. Shi, W. H. Shi, X. H. Rui, Q. Y. Yan, J. Kong, H. Zhang, *Small* **2013**, *9*, 3433 – 3438.
[21] X. Xu, Z. Y. Fan, X. Y. Yu, S. J. Ding, D. M. Yu, X. W. Lou, *Adv. Energy Mater.* **2014**, *4*, 1400902.
[22] H. Liu, D. W. Su, R. F. Zhou, B. Sun, G. X. Wang, S. Z. Qiao, *Adv. Energy Mater.* **2012**, *2*, 970 – 975.
[23] F. Zhou, S. Xin, H. W. Liang, L. T. Song, S. H. Yu, *Angew. Chem. Int. Ed.* **2014**, *53*, 11552 – 11556; *Angew. Chem.* **2014**, *126*, 11736 – 11740.
[24] J. Wang, J. L. Liu, D. L. Chao, J. X. Yan, J. Y. Lin, Z. X. Shen, *Adv. Mater.* **2014**, *26*, 7162 – 7169.
[25] C. B. Zhu, X. K. Mu, P. A. van Aken, Y. Yu, J. Maier, *Angew. Chem. Int. Ed.* **2014**, *53*, 2152 – 2156; *Angew. Chem.* **2014**, *126*, 2184 – 2188.
[26] G. D. Du, Z. P. Guo, S. Q. Wang, R. Zeng, Z. X. Chen, H. K. Liu, *Chem. Commun.* **2010**, *46*, 1106 – 1108.
[27] K. Chang, D. S. Geng, X. F. Li, J. L. Yang, Y. J. Tang, M. Cai, R. Y. Li, X. L. Sun, *Adv. Energy Mater.* **2013**, *3*, 839 – 844.
[28] S. K. Das, R. Mallavajula, N. Jayaprakash, L. A. Archer, *J. Mater. Chem.* **2012**, *22*, 12988 – 12992.
[29] Y. Yan, B. Y. Xia, X. M. Ge, Z. L. Liu, J. Y. Wang, X. Wang, *ACS Appl. Mater. Interfaces* **2013**, *5*, 12794 – 12798.
[30] J. F. Xie, H. Zhang, S. Li, R. X. Wang, X. Sun, M. Zhou, J. F. Zhou, X. W. Lou, Y. Xie, *Adv. Mater.* **2013**, *25*, 5807 – 5813.
[31] X. Y. Yu, L. Yu, L. F. Shen, X. H. Song, H. Y. Chen, X. W. Lou, *Adv. Funct. Mater.* **2014**, *24*, 7440 – 7446.
[32] C. Lei, F. Han, D. Li, W. C. Li, Q. Sun, X. Q. Zhang, A. H. Lu, *Nanoscale* **2013**, *5*, 1168 – 1175.
[33] M. A. Pimenta, E. Del Corro, B. R. Carvalho, C. Fantini, L. M. Malard, *Acc. Chem. Res.* **2015**, *48*, 41 – 47.

Received: March 5, 2015
Published online: May 4, 2015

